Supporting Information

Heterometallic incorporation to promote catalytic activity of polyoxoniobate toward selective oxidation of 5-hydroxymethylfurfural

Lixiao Song, Ziwei Cai, Caili Lv, Longfei Chao, Yundong Cao, Wenjing Xu, Hong Liu*, Chunhui Zhang, Guang-gang Gao**

School of Materials Science and Engineering

University of Jinan

Jinan 250022, China.

*Corresponding authors

E-mail: mse_caoyd@ujn.edu.cn (Yundong Cao); mse_liuh@ujn.edu.cn (Hong Liu); mse_gaogg@ujn.edu.cn (Guanggang Gao)

Experimental Section

1. Materials

All the chemicals and reagents are used as received without any further purification. Dimethylsulfoxide (C_2H_6OS), vanadium oxide (V_2O_5), niobium oxide (Nb_2O_5), copper sulfate pentahydrate ($CuSO_4 \cdot 5H_2O$), potassium hydroxide (KOH), sodium carbonate anhydrous (Na_2CO_3), sodium hydrogen carbonate ($NaHCO_3$), potassium bicarbonate ($KHCO_3$) and potassium carbonate (K_2CO_3) were purchased from China National Pharmaceutical Group Chemical Reagent Co., Ltd. Methanol (CH_3OH), ethanol (C_2H_5OH), acetic acid (CH_3COOH) and acetonitrile (C_2H_3N) were purchased from Merck KGaA. 5-Hydroxymethylfurfural ($C_6H_6O_3$), 5-hydroxymethyl-furan-2-carboxylic acid ($C_6H_6O_4$), furan-2,5-dicarbaldehyde ($C_6H_4O_3$), 5-formyl-2-furoic acid ($C_6H_4O_4$) and 2,5-furandicarboxylic acid ($C_6H_4O_5$) were purchased from Sigma-Aldrich. ethylene diamine anhydrous ($C_2H_8N_2$) were purchased from Aladdin Chemical Co., Ltd.

2. Experimental methods

2.1 Synthesis of $Cu(en)_2SO_4$

The synthesis of $Cu(en)_2SO_4$ was carried out based on previously reported literature [1]. The detailed synthesis procedure was as follows: Prepare a copper sulfate solution ($2mol \cdot L^{-1}$), and mix it with ethylenediamine (en) in a ratio of 1:2 to obtained the dark blue solution. While stirring, slowly add 95% ethanol to the solution until purple fine crystals appear. Then, add the 95% ethanol drop by drop until the volume of ethanol added is approximately 3-4 times that of the original solution. Filtering, followed by washing with anhydrous ethanol and drying. The crystal was placed in a beaker, and a small amount of distilled water was added to immerse the crystal. The mixture was heated to 55 °C to dissolve the crystal. It was then cooled to room temperature and ethanol was added dropwise while stirring until the slightest crystallization just appeared. The beaker was placed in a vacuum drying oven. After 14 h, the beaker was taken out, filtered, washed twice with anhydrous ethanol, then washed with anhydrous ether, and finally dried at 60 °C.

2.2 Synthesis of $K_7[HNb_6O_{19}] \cdot 13H_2O$ (Nb_6)

The synthesis of $K_7[HNb_6O_{19}] \cdot 13H_2O$ was carried out based on previously reported literature [2]. The detailed synthesis procedure was as follows: mix KOH (26 g) and Nb_2O_5 (13.3 g) together and place them in a nickel crucible. Then the mixture was calcined at 450 °C in a tube furnace for 100 minutes. After cooling, dissolve the solid in 100 mL of deionized water, stir for 10 minutes, and then filter. Place the solution in an environment at 0 °C and let it stand for 24 hours. Then, a block-like colorless

crystal will be obtained. The crystals were washed with a small amount of ice-purified water and subsequently dried.

2.3 Synthesis of $[Cu(en)_2]_{3.5}[Cu(en)_2(H_2O)]\{[VNb_{12}O_{40}(VO)_2][Cu(en)_2]\}\cdot 17H_2O$ ($Nb_{12}V_3Cu$)

The synthesis of $[Cu(en)_2]_{3.5}[Cu(en)_2(H_2O)]\{[VNb_{12}O_{40}(VO)_2][Cu(en)_2]\}\cdot 17H_2O$ was carried out based on previously reported literature [3]. The detailed synthesis procedure was as follows: a mixture of 0.15 g $K_7HNb_6O_{19}\cdot 13H_2O$, 0.05 g $NaVO_3$, 0.1 g $CuSO_4\cdot H_2O$ were dispersed in 8 ml of water. Then 10 drops of pure en was added with continuous stir. The pH of the precursor mixture was about 12.3. The mixture was transferred into a 23 ml stainless-steel autoclave and heated at 110 °C for 90 hours. After cooling to room temperature, the block-shaped purple crystals were collected by filtration.

2.4 HPLC analytical methods

In this study, the P3100 high-performance liquid chromatography (HPLC) system was used to analyze the substrate conversion rate, product yield, and selectivity in the catalytic system. The conditions are as follows: analysis was performed using a ZOR-BAX Eclipse XDB-C18 column (4.6 × 150 mm). The mobile phase consisted of acetonitrile and 0.1 wt% aqueous acetic acid (V:V = 15:85). The flow rate was set to 0.5 mL min^{-1}, the column temperature was maintained at 30 °C, and the UV detector was set to a wavelength of 280 nm. After filtering the reaction solution, transfer 500 μL of it into a 50 mL volumetric flask and dilute to the mark with deionized water. The content of HMF, DFF, HMFCA, FFCA and FDCA in the sample was determined using the external standard method with calibration curves from standards. Then, the conversion rate of HMF, product yield, and selectivity were calculated using the following formulas:

$$\text{HMF conversion (\%)} = \frac{\text{mol of converted HMF}}{\text{mol of initial HMF}} \times 100\%$$

$$\text{Product yield (\%)} = \frac{\text{mol of obtained product}}{\text{mol of initial HMF}} \times 100\%$$

3. Experimental Section

3.1 Characterization methods

The morphologies of the samples were analyzed using TEM (JEM-2100F, 200 kV) equipped with an energy dispersive X-ray spectroscopy. The structures of the samples were identified using X-ray diffraction (XRD, Rigaku SmartLab 9KW) with Cu Kα radiation. The XPS spectra were detected by a ESCALAB-MKII spectrometer (VG Co., UK) with Al Kr X-ray radiation as the X-ray source for excitation. FTIR spectra were obtained using a NEXUS-870 spectrometer with KBr pellets. The products from catalytic reaction were analyzed by high-performance liquid chromatography (Elite EC1assical 3100 HPLC) using a reversed-phase ZOR-BAX Eclipse XDB-C18 column (4.6 × 150 mm) with UV detection (280 nm) and an SPD-20A UV detector. UV-vis diffuse reflectance spectra were measured using a Shimazu UV-visible spectrophotome ter UV-8000. The solid samples were ground and crushed before testing. Background calibration and baseline calibration were performed on the instrument before sample testing. Raman testing was performed using a Raman spectrometer (Labramis, Horiba Jobbin Yvon, Paris, France).

3.2 Computation methods

The calculation is carried out within the DFT framework, using the Dmol3 module in the Materials Studio software package for structural optimization. The function PBE, belonging to the Gradient-based (GGA), is used to process the exchange correlation potential energy. The Core treatment is DFT Semi-core Pseudopots. The

Basis set is DNP. A cut-off energy of 400 eV was used for the plane-wave basis to ensure convergence. For geometric optimization, the atomic positions are fully relaxed until the residual forces on constituent atoms become less than 0.02 eV $Å^{-1}$. Herein, the binding energy

(E_a) is defined as:

$$E_b = E_{total} - E_{ads} - E_{sub}$$

Where E_{total} is the total energy of the adsorbed system, E_{ads} and E_{sub} are the energy of the adsorbate in vacuum, respectively [4-5].

The Gibbs free energy changes (ΔG) of the reaction are calculated using the following formula:

$$\Delta G = \Delta E + \Delta ZPE - T\Delta S$$

Where ΔE is the electronic energy difference directly obtained from DFT calculations, ΔZPE is the zero-point energy difference, T is the room temperature (298.15 K) and ΔS is the entropy change.

The adsorption energies (E_{ads}) of a molecule are calculated by:

$$E_{ads} = E_{*A} - E_A - E_{Sub}$$

Where E_A and E_{*A} represent the energies before and after the adsorption of a molecule on the substrate, respectively. E_{sub} is the energy of clean surface.

4. Supporting figures

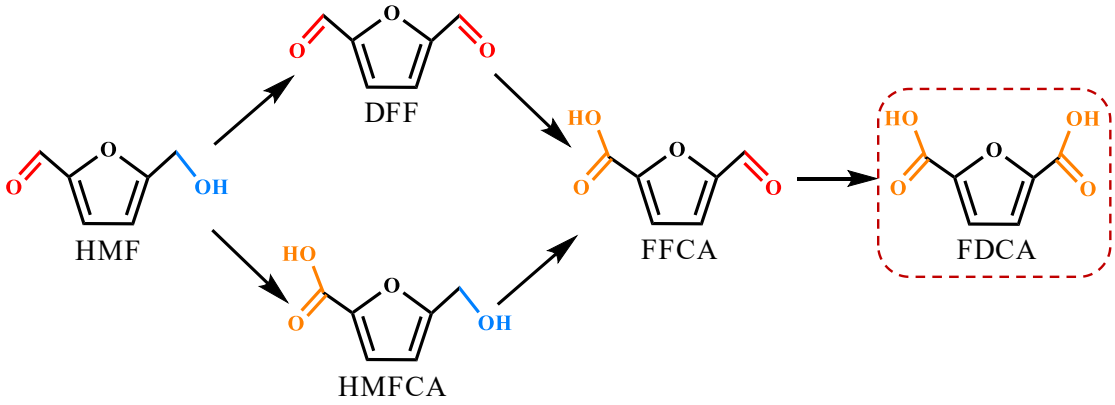

Fig. S1. Possible oxidative routes for HMF conversion. 5-Hydroxymethylfurfural (HMF), 2,5-Diformylfuran (DFF), 5-Methyl-2-furancarboxylic acid (FFCA), 2,5-Furandicarboxylic acid (FDCA), 5-Hydroxymethyl-2-furancarboxylic acid (HMFCA).

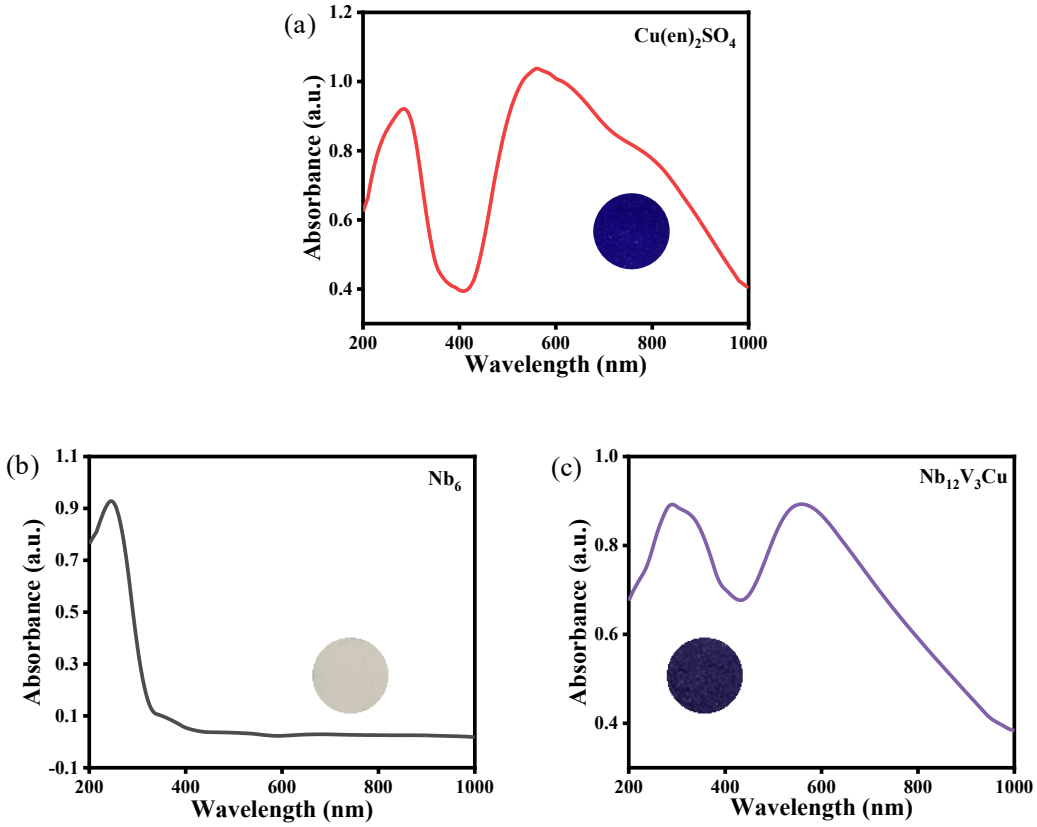

Fig. S2. UV-vis spectra of $Cu(en)_2SO_4$ (a), Nb_6 (b) and $Nb_{12}V_3Cu$ (c) (the insets are the photographs of catalysts).

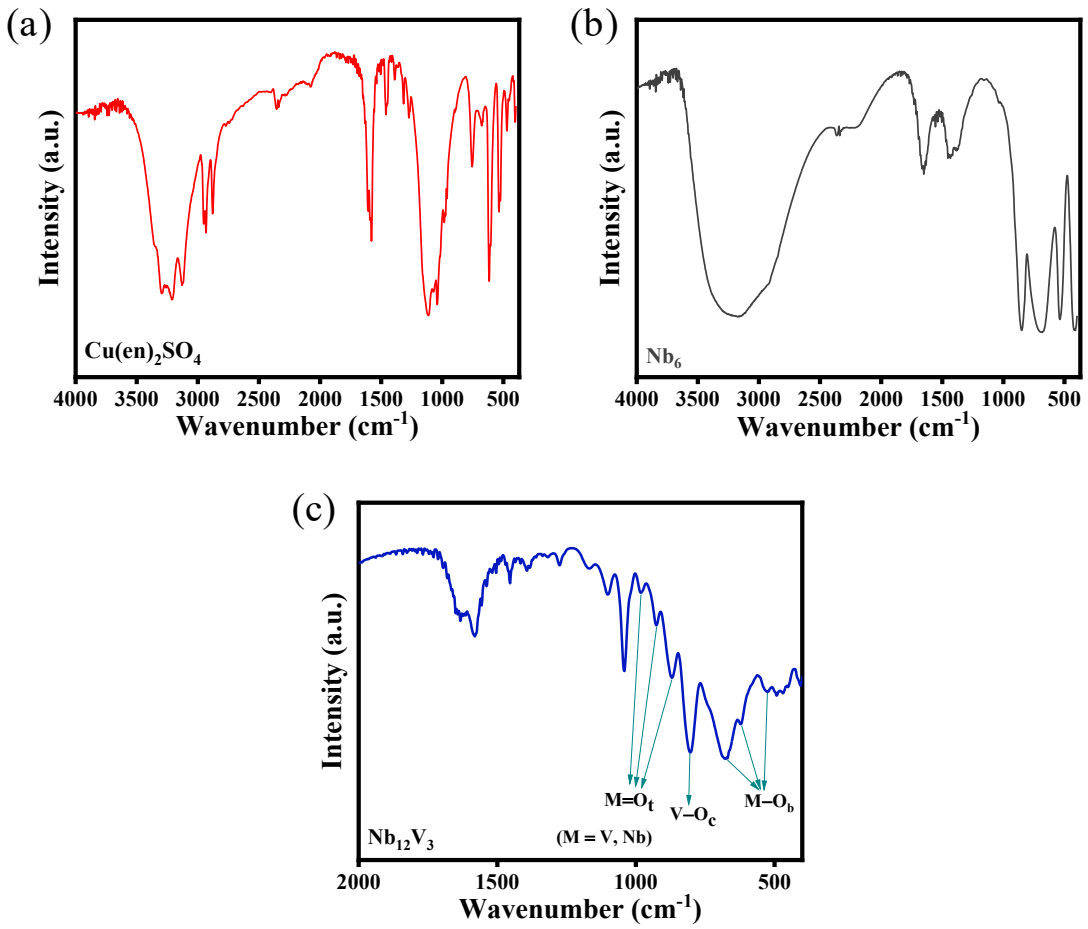

Fig. S3. FTIR spectra of $Cu(en)_2SO_4$ (a), Nb_6 (b) and $Nb_{12}V_3Cu$ (c).

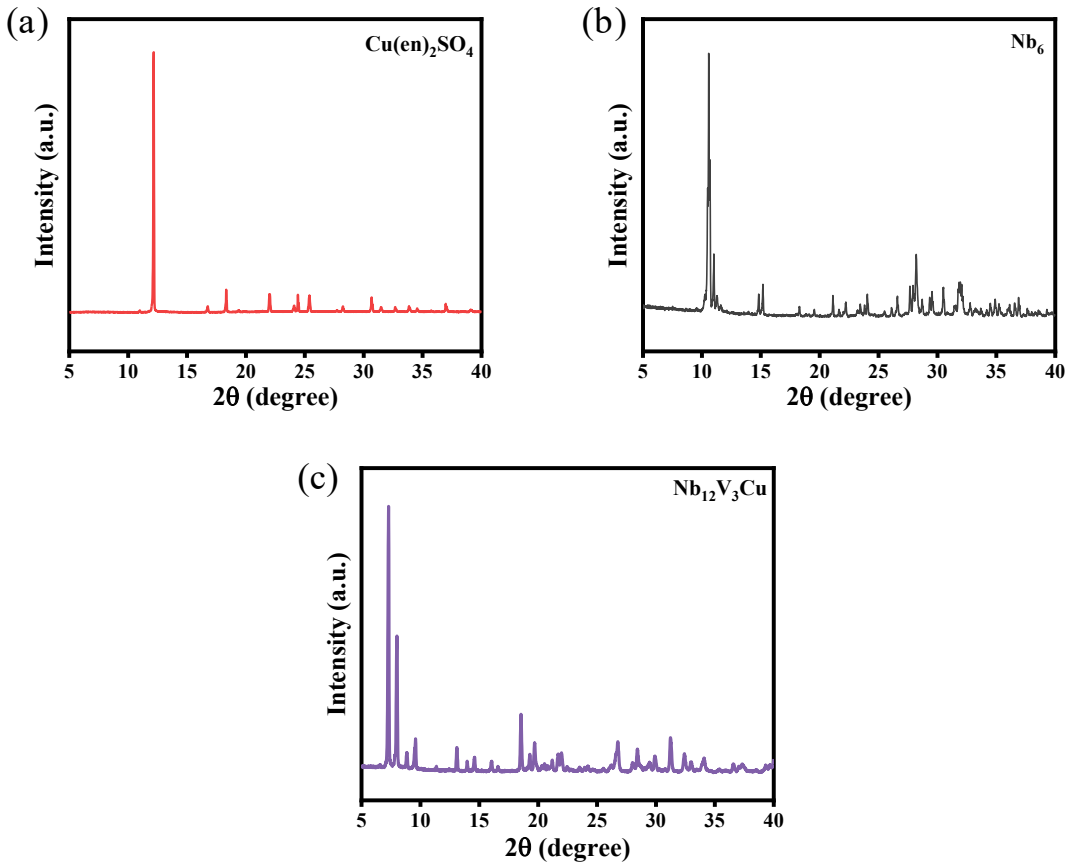

Fig. S4. PXRD patterns of $Cu(en)_2SO_4$ (a), Nb_6 (b) and $Nb_{12}V_3Cu$ (c).

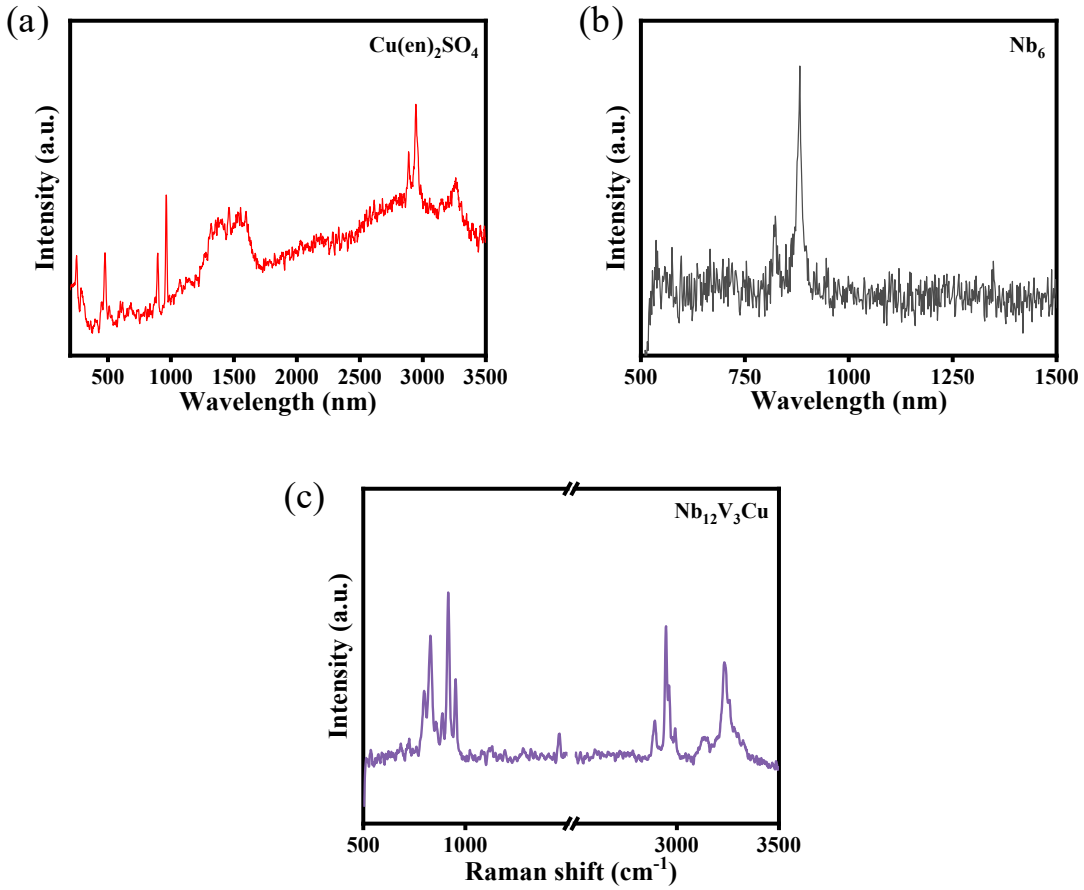

Fig. S5. Raman spectra of $Cu(en)_2SO_4$ (a), Nb_6 (b) and $Nb_{12}V_3Cu$ (c).

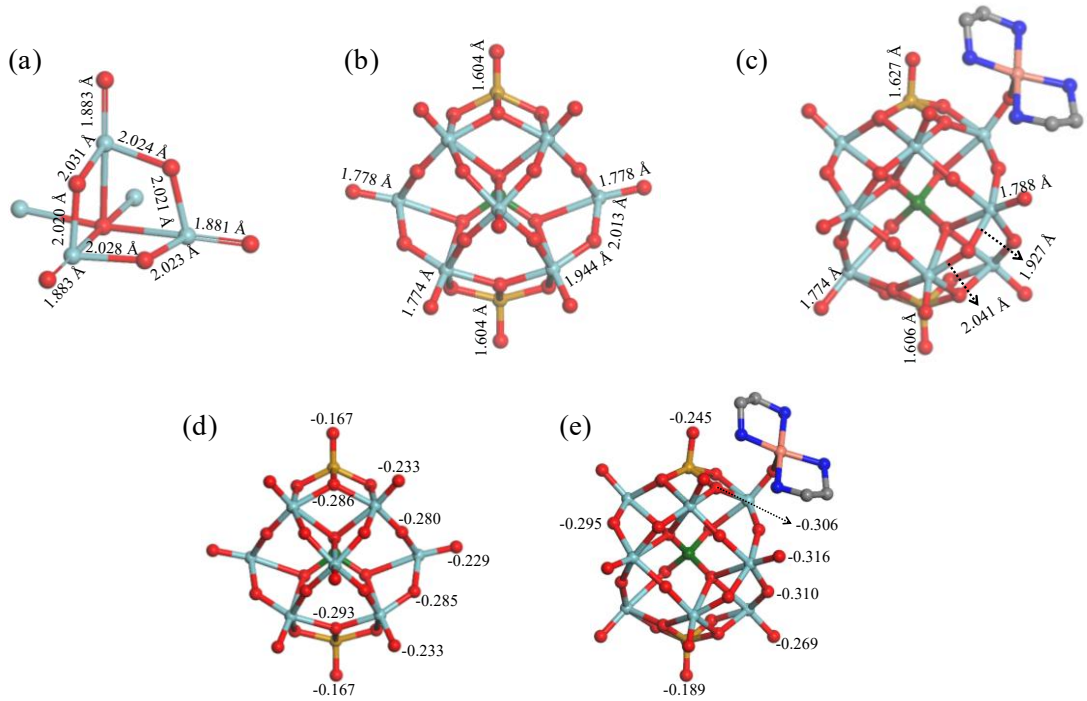

Fig. S6. A portion of bond lengths of O_b and O_t in Nb_6 (a), $[VNb_{12}(VO)_2]^{11-}$ (b), and $Nb_{12}V_3Cu$ (c). Hirshfeld charges of O_b and O_t in $[VNb_{12}(VO)_2]^{11-}$ (d), and $Nb_{12}V_3Cu$ (e) (some oxygen atoms were omitted for clarity).

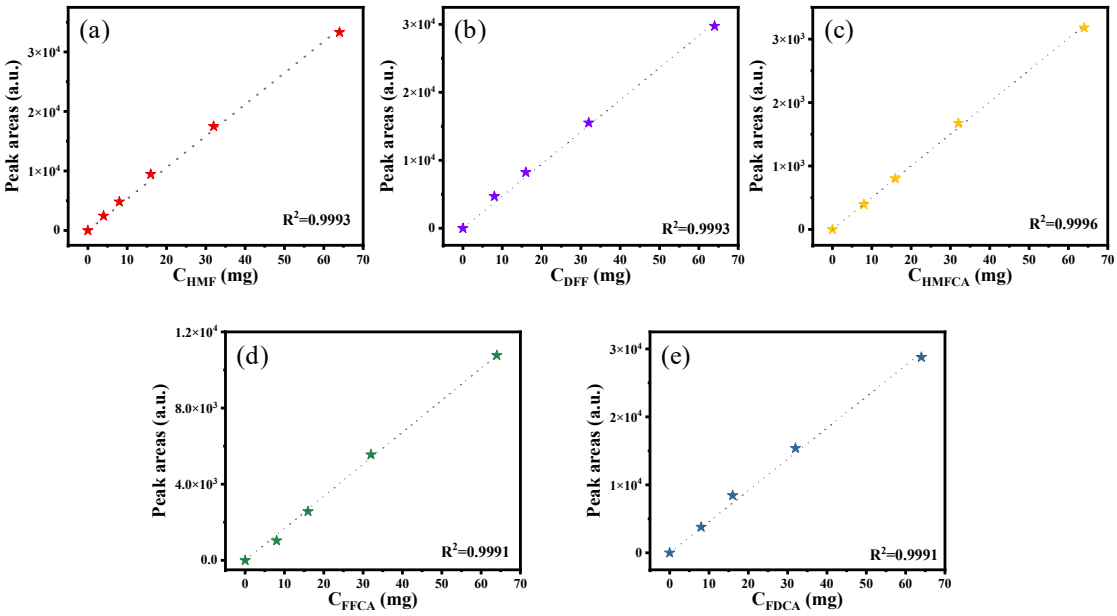

Fig. S7. Standard curves of HMF (a), DFF (b), HMFCA(c), FFCA (d), and FDCA (e).

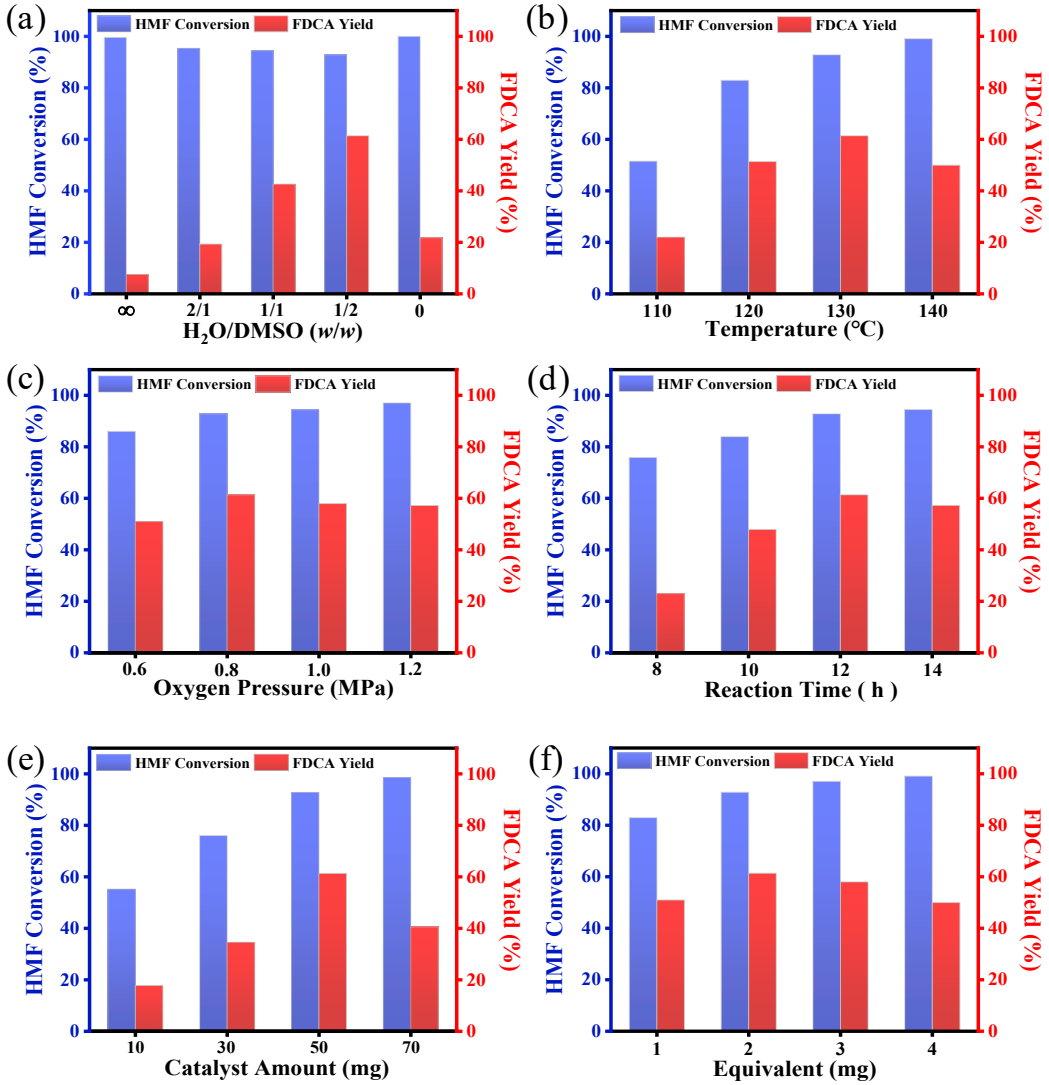

Fig. S8. The effect of reaction conditions on HMF oxidation over Nb_6: the ratio of H_2O/DMSO (a), temperature (b), oxygen pressure (c), reaction time (d), catalyst amount (e), alkali additive dosage (f). Reaction conditions: HMF (40 mg), $KHCO_3$ (70 mg), solvent (6 mL).

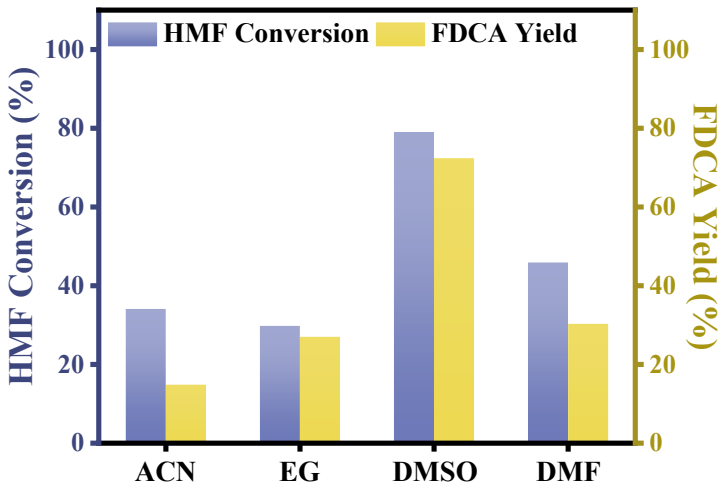

Fig. S9. The catalytic performance of $Nb_{12}V_3Cu$ in different organic solutions. Reaction conditions: HMF (40 mg), catalyst (10 mg), $KHCO_3$ (70 mg), 110 °C, 6 h, O_2 pressure (0.8 MPa), solvent (6 mL).

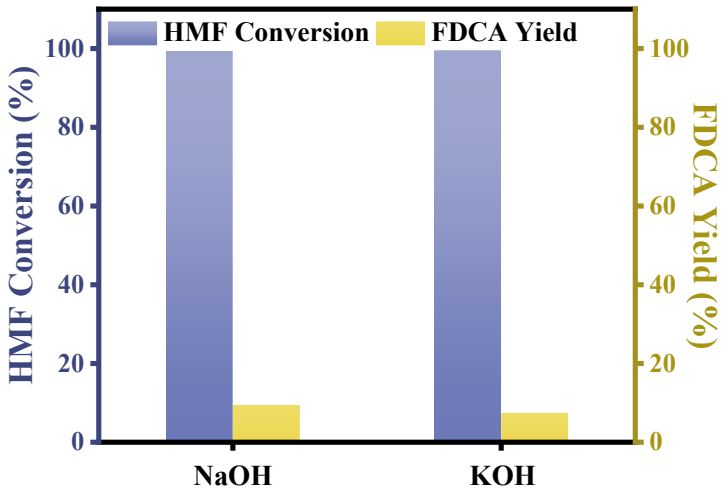

Fig. S10. The catalytic oxidation performance of $Nb_{12}V_3Cu$ when NaOH and KOH are used as alkaline additives. Reaction conditions: HMF (40 mg), catalyst (10 mg), alkaline additive (70 mg), 110 °C, 6 h, O_2 pressure (0.8 MPa), H_2O/DMSO mass ratio = 1:3 (6 mL total solvent).

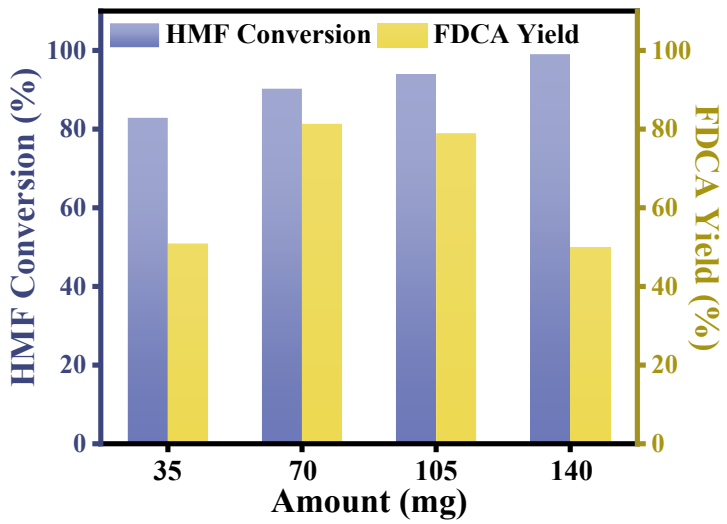

Fig. S11. The influence of different addition amounts of $KHCO_3$ on the catalytic performance of $Nb_{12}V_3Cu$.

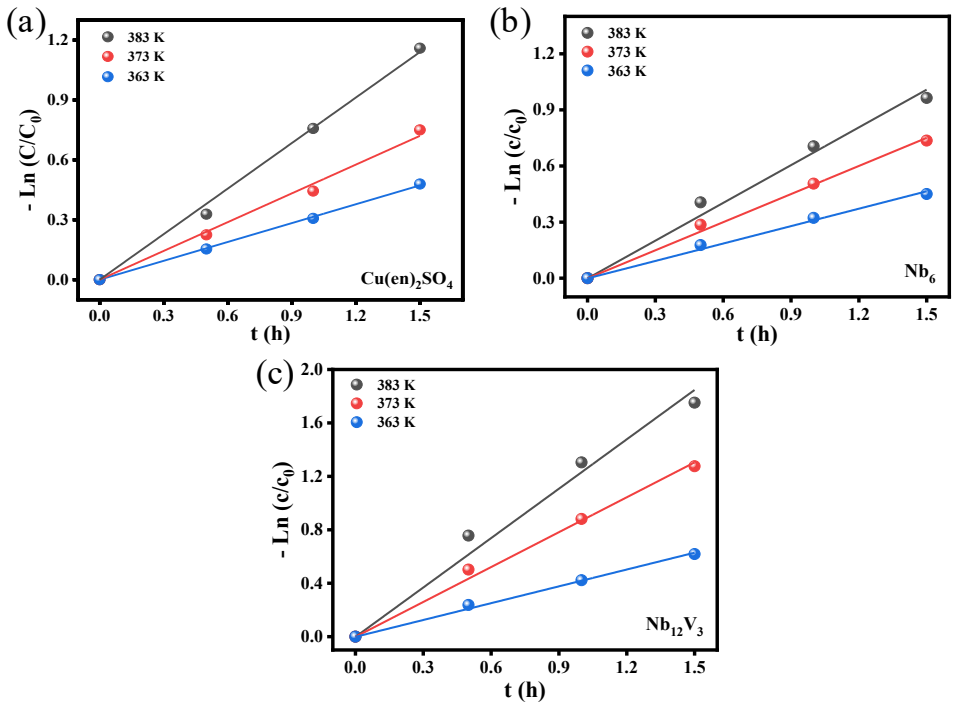

Fig. S12. Fitting of pseudo-first-order kinetic model to the HMF oxidation reaction data collected over different catalysts: $Cu(en)_2SO_4$ (a); Nb_6 (b); $Nb_{12}V_3Cu$ (c). Reaction conditions: HMF (40 mg), catalyst (10 mg), $KHCO_3$ (70 mg), O_2 pressure (0.8 MPa), H_2O/DMSO mass ratio = 1:3 (6 mL total solvent).

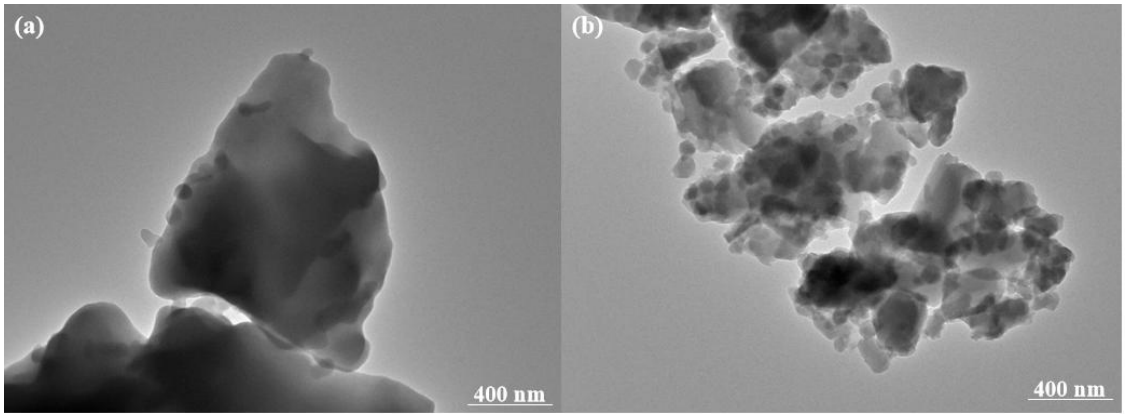

Fig. S13. The TEM images of $Nb_{12}V_3Cu$ before (a) and after (b) reaction.

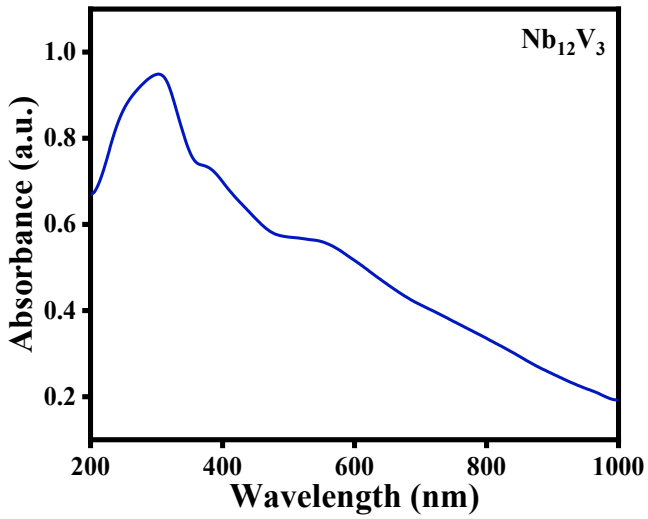

Fig. S14. UV-Vis DRS spectra of $Nb_{12}V_3Cu$ after the reactions.

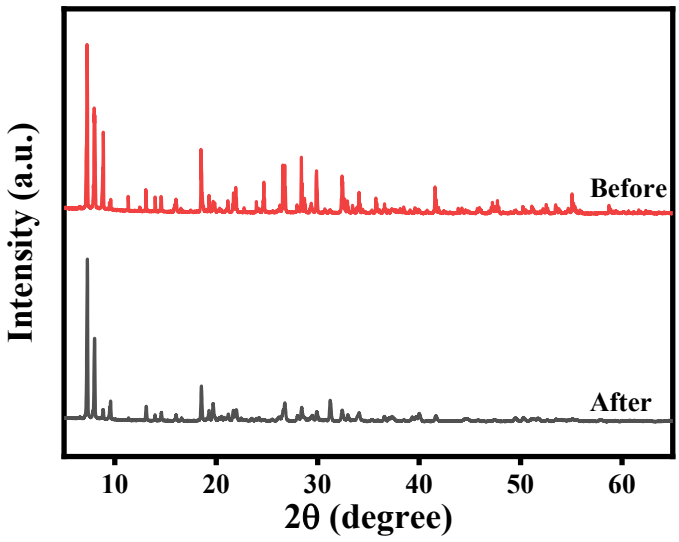

Fig. S15. XRD patterns of $Nb_{12}V_3Cu$ before and after the reaction.

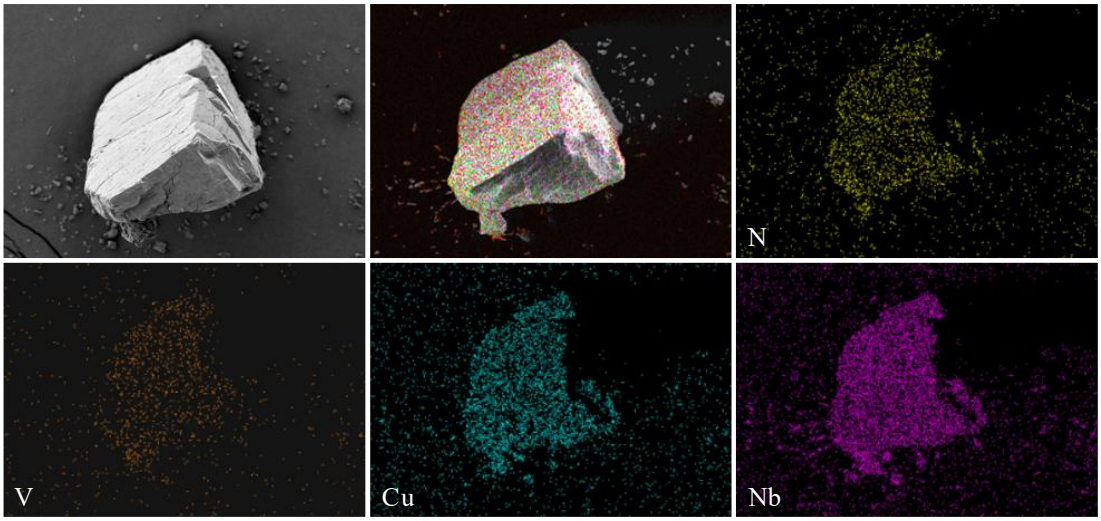

Fig. S16. SEM and elemental mapping of the $Nb_{12}V_3Cu$ after catalytic process.

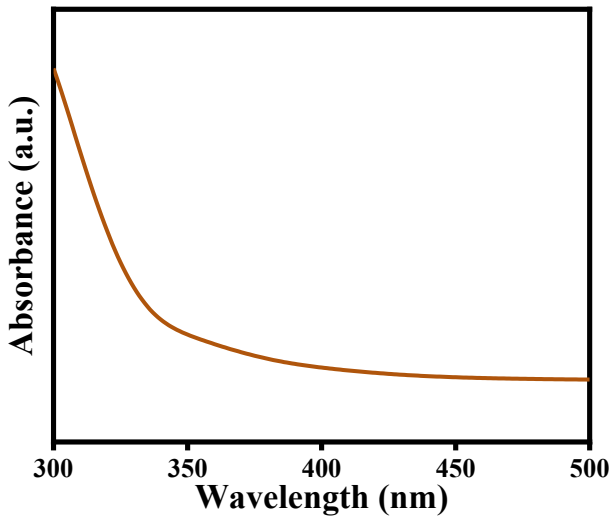

Fig. S17. H_2O_2 detection during the HMF oxidation.

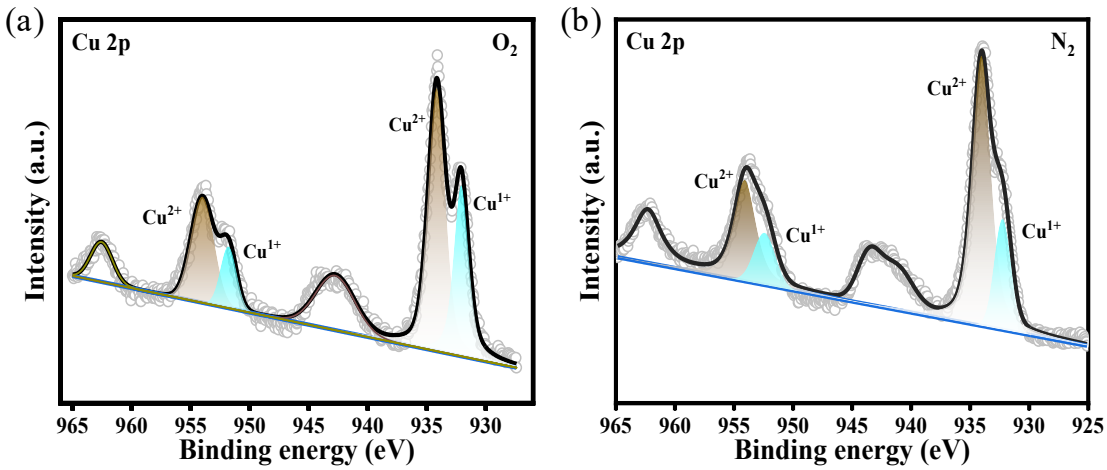

Fig. S18. Cu 2p XPS analyses of $Cu(en)_2SO_4$ after reaction under O_2 (a) and N_2 (b).

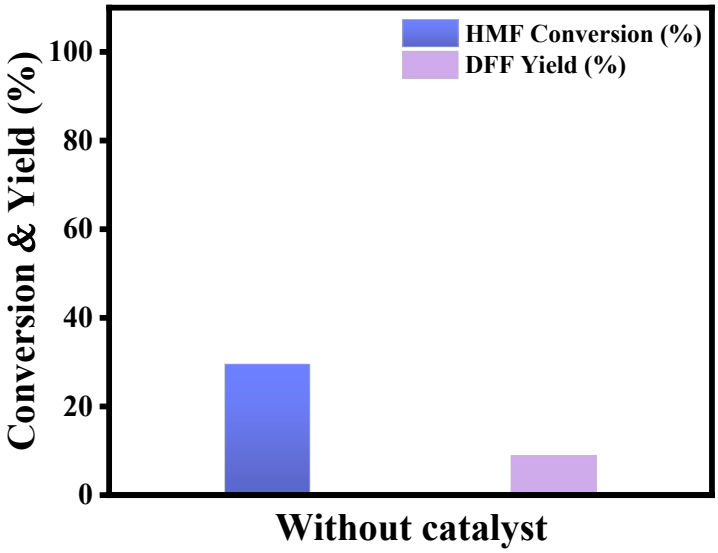

Fig. S19. The catalytic performance of HMF without catalyst. Reaction conditions: HMF (40 mg), $KHCO_3$ (70 mg), 110 °C, 6 h, O_2 pressure (0.8 MPa), H_2O/DMSO mass ratio = 1:3 (6 mL total solvent).

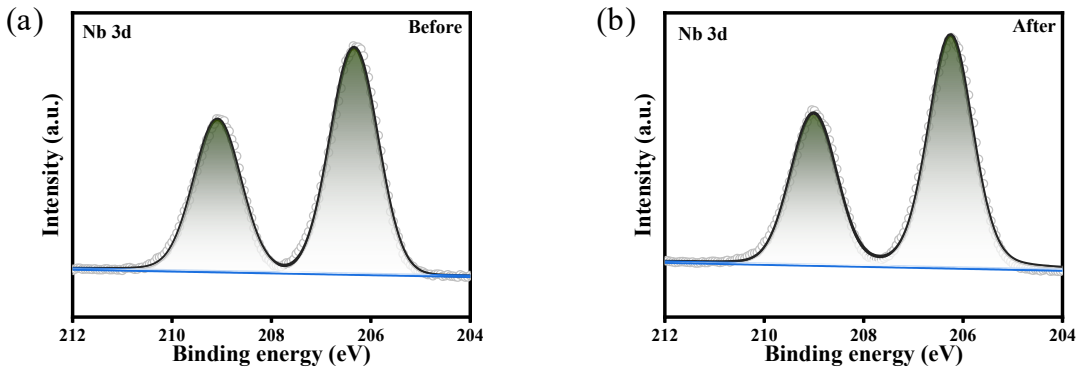

Fig. S20. Nb 3d XPS analyses of Nb_6 before (a) and after (b) reaction under O_2.

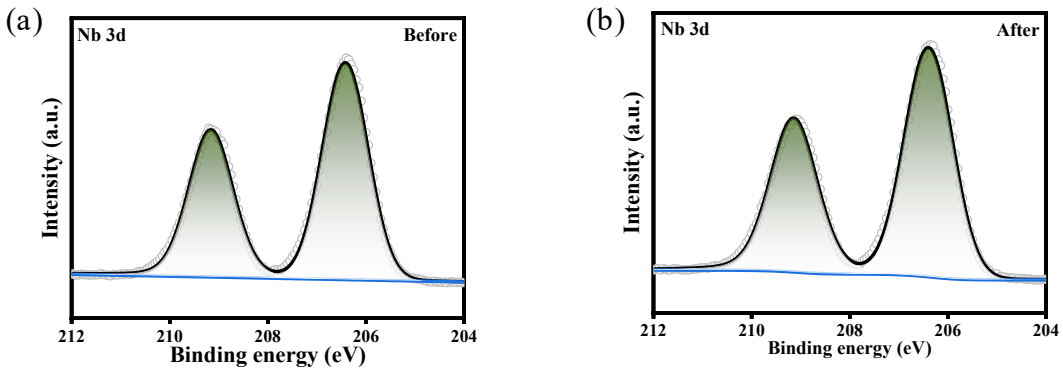

Fig. S21. Nb 3d XPS analyses of $Nb_{12}V_3Cu$ before (a) and after (b) reaction under O_2.

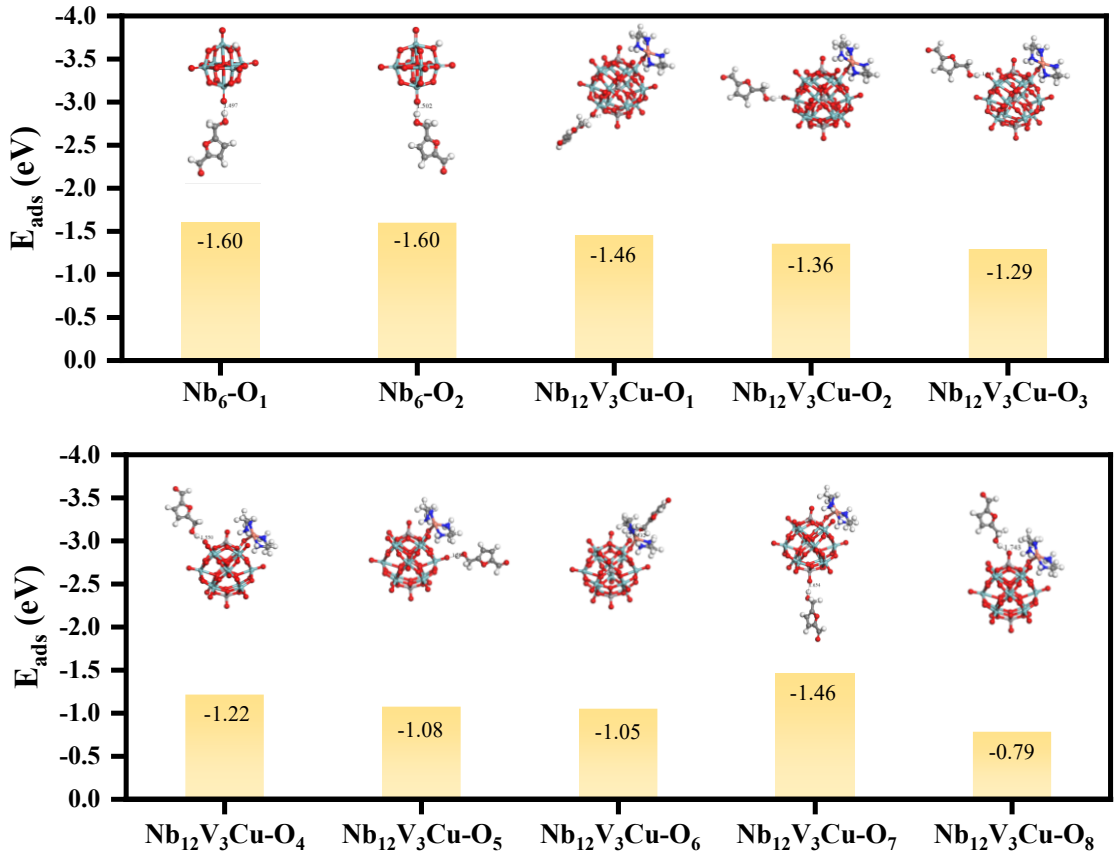

Fig. S22. The interaction energies of different terminal oxygen sites with the terminal hydrogen atoms of HMF.

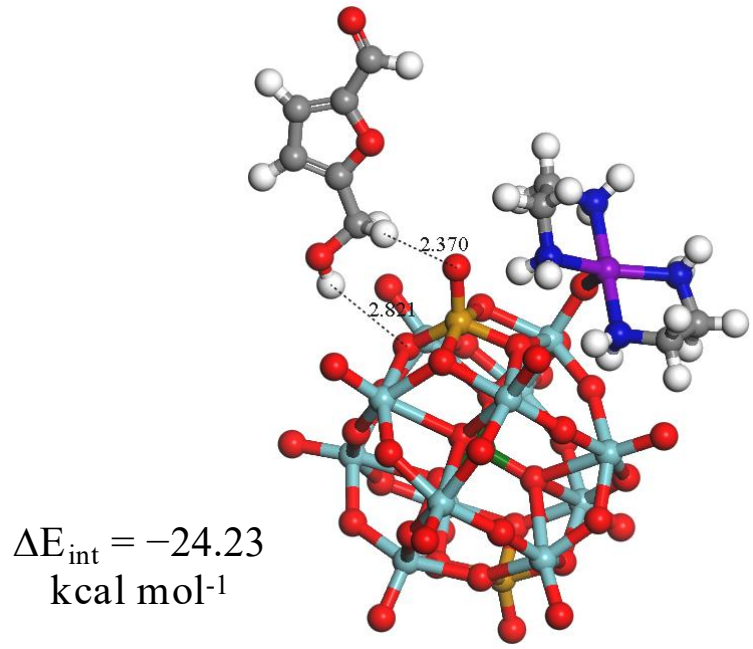

Fig. S23. Structure, interaction energy (ΔE_{int}) in $Nb_{12}V_3Cu$-V_2-O_b binding mode.

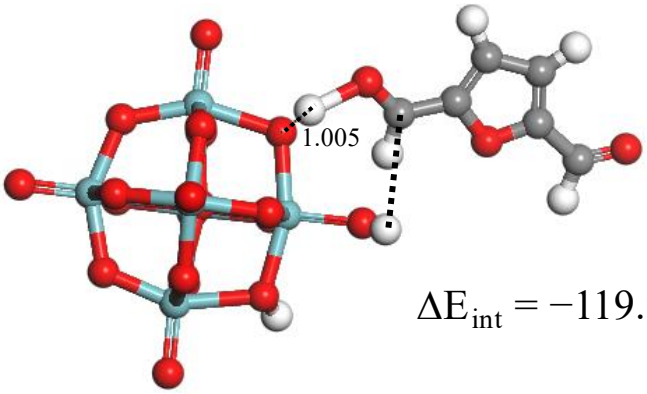

Fig. S24. Structure, interaction energy (ΔE_{int}) in Nb_6-O_b binding mode.

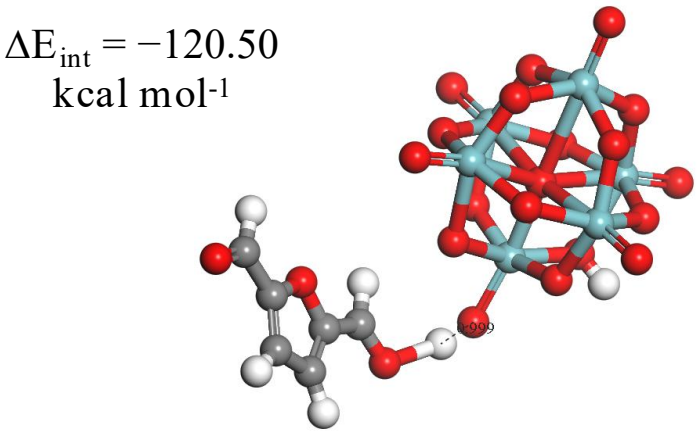

Fig. S25. Structure, interaction energy (ΔE_{int}) in Nb_6-O_t binding mode.

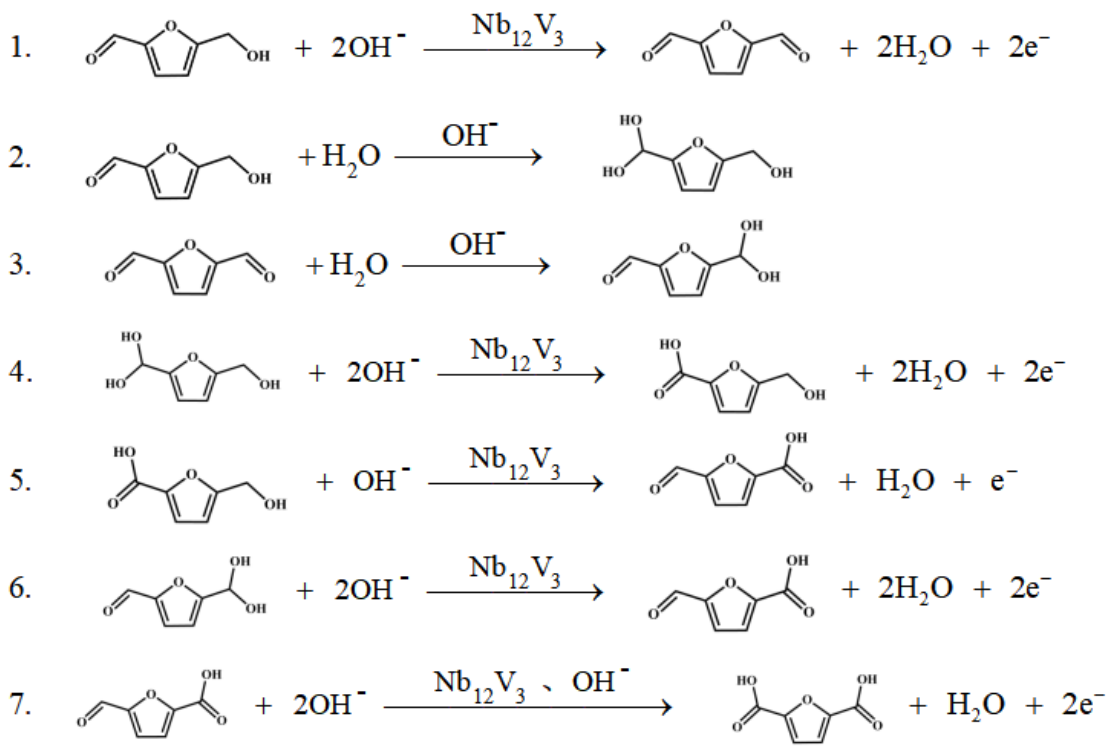

Fig. S26. Overall mechanism of HMF oxidation to FDCA over the $Nb_{12}V_3Cu$.

5. Supporting tables

Table S1. Comparison of $Nb_{12}V_3Cu$ and other catalysts on selective oxidation of HMF to FDCA.

Index	Catalyst	Solvent	Type	base	t (h)	T (℃)	TON	TOF (h^{-1})	HMF Conv.(%)	FDCA yield (%)	Ref.
1	CuO/ZSM-5	H2O	Heterogeneous	K_2CO_3	5	130	10	2	80	70	3
2	[EMIM]Mo8	H2O	Homogeneous	NaOH	2	90	10	5	95.2	89.18	54
3	—	H2O	—	NaOH	2	70	—	—	98	49.7	54
4	Co-Fe-P-400/ LDH	ACN	Heterogeneous	—	6	80	NR	—	66	6.6	70
5	NiCo2O4	ACN/TBHP	Heterogeneous	—	12	80	10.4	0.87	100	60	71
6	PMo6V6	[Bmim]Cl	Homogeneous	—	6	140	3.12	0.52	99	88	53
7	—	[Bmim]Cl	—	—	6	140	—	—	99.2	18.7	53
8	PMo6V6	DMSO	Homogeneous	—	6	140	3.12	0.52	100	0.1	53
9	Pt/C	H2O/DMSO	Heterogeneous	K_2CO_3	6	75	NR	—	55.3	6	17
10	this work	H2O/DMSO	Homogeneous	$KHCO_3$	6	110	98.77	16.46	90.3	81.4	—

Table S2. The interaction energies between the hydroxyl group of HMF and distinct oxygen species within the Nb_6 clusters, along with the activated bond lengths variation (Δd) for O–H (Δd_{OH}), C–H (Δd_{CH}), and H···O interactions (specifically H···O_t or H···O_b).

System	ΔE_{int} (kcal mol^{-1})	Δd_{OH} (Å)	Δd_{CH} (Å)	H···O_t (or O_b) (Å)
Nb-O_t	−120.50	0.734	2,039	0.999
Nb-O_b	−119.90	0.717	2.640	1.005

6. References

[1] Baldwin ME. Complexes of cupric sulfate with ethylenediamine. Spectrochim Acta 1963;19:315-320. https://doi.org/10.1016/0371-1951(63)80110-1.

[2] Filowitz M, Ho RKC, Klemperer WG, Shum W. Oxygen-17 nuclear magnetic resonance spectroscopy of polyoxometalates. 1. sensitivity and resolution. Inorg Chem 1979;18:93-103. https://doi.org/10.1021/ic50191a021.

[3] Gou GL, Xu YQ, Cao J, Hu CW. An unprecedented vanadoniobate cluster with 'trans-vanadium' bicapped Keggin-type $\{VNb_{12}O_{40}(VO)_2\}$. Chem Commun 2011;47:9411-9413. https://doi.org/10.1039/C1CC12329G.

[4] Humphrey W, Dalke A, Schulten K. VMD: Visual molecular dynamics. J Mol Graph 1996;14:33-38. https://doi.org/10.1016/0263-7855(96)00018-5.

[5] Lu T, Chen FW. Multiwfn: A multifunctional wavefunction analyzer. J Comput Chem 2012;33:580. https://doi.org/10.1002/jcc.22885.